

Thermochemical structures within a spherical mantle: Superplumes or piles?

Allen K. McNamara and Shijie Zhong

Department of Physics, University of Colorado, Boulder, Colorado, USA

Received 14 October 2003; revised 9 March 2004; accepted 1 June 2004; published 20 July 2004.

[1] Heterogeneous compositional mantle models are frequently invoked to explain some observations obtained from geochemistry and seismology. In particular, two regions in the Earth's lower mantle, under the Pacific and Africa, are often interpreted as being either piles or superplumes of dense material. We perform numerical modeling of thermochemical convection in a three-dimensional spherical geometry to investigate whether the geometry can focus a dense chemical component into a small number of isolated, rounded piles or superplumes of material. We study the effect of temperature and compositionally dependent viscosity, and we find two different modes of dense layer deformation. Temperature-dependent rheology leads to a low-viscosity dense layer which is passively swept aside by downwellings into linear piles that are spread throughout the entire lower mantle. The addition of compositionally dependent rheology in which the dense layer is more viscous results in active deformation of the dense material, forming large, isolated superplumes. Our results indicate that piles and superplumes are separate features which, in general, do not occur together and, in order for isolated, rounded superplumes to form, an intrinsic compositional viscosity increase is required for the dense material.

INDEX TERMS: 8121 Tectonophysics: Dynamics, convection currents and mantle plumes; 8162 Tectonophysics: Rheology—mantle; 8147 Tectonophysics: Planetary interiors (5430, 5724); 8124 Tectonophysics: Earth's interior—composition and state (1212); 8199 Tectonophysics: General or miscellaneous; *KEYWORDS:* thermochemical convection, superplumes, spherical geometry

Citation: McNamara, A. K., and S. Zhong (2004), Thermochemical structures within a spherical mantle: Superplumes or piles?, *J. Geophys. Res.*, 109, B07402, doi:10.1029/2003JB002847.

1. Introduction

[2] Heterogeneous compositional mantle models are frequently invoked [e.g., Kellogg *et al.*, 1999] to explain some characteristics of seismological studies that hint at lateral variations in wave speed that cannot be explained by thermal effects alone [van der Hilst and Karason, 1999; Masters *et al.*, 2000]. In particular, two regions in the Earth's lower mantle appear to require a distinct chemical component: under the Pacific and Africa [Su and Dziewonski, 1997; Ishii and Tromp, 1999; Ni *et al.*, 2002; Romanowicz and Gung, 2002; Ni and Helmberger, 2003a, 2003b]. Large-scale low seismic velocities in these regions and the anomalous superswell surface topography above them [McNutt, 1998] are commonly associated with the presence of chemical superplumes originating from the core-mantle boundary [e.g., Tackley, 1998; Davaille, 1999].

[3] Moreover, geochemical differences between mid-ocean ridge basalts and ocean island basalts are more easily explained by a heterogeneous mantle chemistry with different source regions [e.g., Hofmann, 1997]; however, recent work by Meibom *et al.* [2003] argues against some of these geochemical constraints. In addition, geophysical

arguments based on the Earth's heat budget imply a deep reservoir in which excess heat may be retained over geological times.

[4] Models based on distinct radial chemical layers of material have generally fallen out of favor because of seismological evidence of slabs successfully reaching the core-mantle boundary (CMB) [Grand *et al.*, 1997; van der Hilst *et al.*, 1997; Bijwaard *et al.*, 1998], geophysical arguments based on plume flux [Davies and Richards, 1992], and numerical models illustrating the very high temperature contrast between layers [Spohn and Schubert, 1982; McNamara and van Keken, 2000; Tackley, 2002]. As a result, several models which attempt to overcome these problems have been proposed. One such model involves a slightly more dense enriched layer at the base of the mantle which is allowed to undulate significantly, allowing slabs to nearly reach the CMB [Kellogg *et al.*, 1999]. Other solutions include blobs of more viscous material [Becker *et al.*, 1999] or piles of dense material under the Pacific and Africa [Tackley, 1998].

[5] Several numerical and laboratory studies have been performed in three-dimensional (3-D) Cartesian geometries to study the effect that a dense mantle component has on the style of convection. Of particular interest is how the interface between the components deforms. Numerical studies [Tackley, 1998, 2002] in which a dense component

has similar or lower viscosity than the less dense material reveal that the dense material tends to be swept around by convection occurring in the less dense material. Dense material is pushed aside by downwellings and is swept into an interconnected network of linear piles beneath upwelling regions. This same type of behavior has been observed in laboratory studies [Olson and Kincaid, 1991]. Entrainment of dense material occurs along the linear piles, gradually depleting the dense component, a common feature of laboratory studies as well [e.g., Olson, 1984]. Tackley [2002] speculates that a spherical geometry may lead to a flow structure that sweeps the dense material into rounded piles as opposed to the linear ones generated in 3-D Cartesian models.

[6] Extensive laboratory studies of thermochemical convection have been performed by Davaille [1999] and Davaille *et al.* [2002, 2003] in a 3-D Cartesian system. They categorize their results into two different flow regimes: whole layer and stratified. The whole layer regime occurs for small density contrasts and is characterized by large-scale undulations of the interface between chemical components. In this regime the thermal buoyancy of the dense material overcomes its intrinsic negative buoyancy, and as a result, large domes of the dense material form and rise to the top of the model. They find that the direction of doming is controlled by the viscosity contrast between materials and the initial layer thickness. This regime is further divided into overturning and oscillating categories on the basis of whether the dense material maintains its integrity or quickly mixes with the less dense material. In the oscillating category the rising domes cool as they rise, losing their thermal buoyancy. They eventually sink to the bottom of the model with little mixing. The number of oscillations before complete mixing of the materials depends on the viscosity and thickness ratios of the components. They suggest that domes formed in the oscillating regime may be the cause of observed superswells under the Pacific and Africa. The stratified regime occurs for large density contrasts and is characterized by a relatively flat interface between layers in which each layer of material convects separately. Entrainment along cusps formed at the interface occurs, however, allowing the development of thermochemical plumes.

[7] Whereas the experiments of Davaille [1999] and Davaille *et al.* [2002, 2003] employ a higher-viscosity dense material, Jellinek and Manga [2002] performed a series of experiments in which they injected a low-viscosity dense material at the base of their model. They observed that the dense material organized itself into divides formed between circular holes or embayments. The morphology of this interface was not unlike that observed in the numerical results of Tackley [1998, 2002], in which the dense material forms a system of ridges.

[8] The purpose of this work is to study how a 3-D spherical geometry affects the morphology of a dense layer in the lower mantle. We are specifically interested in investigating whether the spherical geometry promotes the development of a small number of rounded piles of dense material, as is often inferred from seismic observations. We also look into the role that temperature-dependent and compositionally dependent rheology plays in generating thermochemical structures. This work is meant to comple-

ment previous laboratory studies by including characteristics that are difficult, if not impossible, to reproduce in fluid dynamics experiments such as temperature-dependent rheology, heat production, and the 3-D spherical geometry.

[9] Our results reveal a distinction between pile and superplume structures. When employing a temperature-dependent rheology alone, we find that the spherical geometry fails to sweep the low-viscosity dense material into rounded piles. Rather, the dense material is passively swept into linear piles surrounding downwelling regions, as shown in previous 3-D Cartesian studies [e.g., Tackley, 1998, 2002]. The inclusion of an intrinsic compositional viscosity increase in the dense material, however, causes the dense material to take a more active role and results in the formation of a small number of isolated, rounded plume structures.

2. Method

2.1. Governing Equations

[10] The numerical calculations are performed by solving the nondimensional conservation equations of mass, momentum, and energy in the Boussinesq approximation. The equation for mass conservation in incompressible flow is

$$\nabla \cdot \mathbf{u} = 0, \quad (1)$$

where \mathbf{u} is the velocity vector. The momentum equation is

$$-\nabla P + \nabla \cdot (\eta \dot{\epsilon}) = (RaT - RbC)\hat{\mathbf{r}}, \quad (2)$$

where $\hat{\mathbf{r}}$ is the radial unit vector, P is the dynamic pressure, η is the viscosity, $\dot{\epsilon}$ is the strain rate tensor, T is the temperature, C is the composition, and Ra is the thermal Rayleigh number defined as

$$Ra = \frac{\alpha \rho g \Delta T h^3}{\eta \kappa}, \quad (3)$$

where α is the thermal expansivity, ρ is the density, g is the acceleration of gravity, ΔT is the temperature drop across the mantle, h is the mantle thickness, and κ is the thermal diffusivity.

[11] Rb is the chemical Rayleigh number defined as

$$Rb = \frac{\Delta \rho g h^3}{\eta \kappa}, \quad (4)$$

where $\Delta \rho$ is the density contrast between chemical components. A useful nondimensional quantity is the buoyancy ratio, B , which is the ratio of chemical to thermal buoyancy:

$$B = \frac{Rb}{Ra} = \frac{\Delta \rho}{\rho \alpha \Delta T}. \quad (5)$$

The energy equation is expressed as

$$\frac{\partial T}{\partial t} + (\mathbf{u} \cdot \nabla)T = \nabla^2 T + H, \quad (6)$$

Table 1. Thermochemical Calculations^a

Case	Input Parameters							Figure	Snapshot Characteristics			
	Ra	Δd	B	A	η_c	H_d	H_l		Time Step	t'	Transit Times	v_{surf}
1	4.8×10^6	0.15	0.7	0.0	0.0	10	10	1a, 1c, 1e	4,000	1.40×10^{-2}	5.70	408
2	4.8×10^6	0.15	0.8	0.0	0.0	10	10	1b, 1d, 1f	3,800	1.32×10^{-2}	5.43	413
3	4.8×10^6	0.10	0.8	6.9	0.0	10	10	2a–2c	8,000	2.23×10^{-2}	3.57	160
4	4.8×10^6	0.10	0.7	6.9	0.0	10	10	3a–3d	6,000	1.49×10^{-2}	2.91	196
5	4.8×10^6	0.10	0.6	6.9	0.0	10	10	3e	2,000	3.73×10^{-3}	0.88	235
6	4.8×10^6	0.15	0.8	6.9	0.0	10	10	4a	11,000	2.22×10^{-2}	4.11	185
7	4.8×10^6	0.15	0.7	6.9	0.0	10	10	4b	11,000	2.22×10^{-2}	3.58	161
8	4.8×10^6	0.15	0.6	6.9	0.0	10	10	4c	5,000	8.43×10^{-3}	1.51	180
9	4.8×10^6	0.10	0.7	9.2	0.0	10	10	4d	9,000	1.23×10^{-2}	2.44	199
10	4.8×10^6	0.10	0.8	6.9	0.0	50	10	4e	10,000	3.07×10^{-2}	6.24	204
11	4.8×10^6	0.10	0.7	6.9	100.0	10	10	5a–5c	6,000	4.85×10^{-2}	8.84	182
11	4.8×10^6	0.10	0.7	6.9	100.0	10	10	5d	20,000	1.33×10^{-1}	29.73	224
12	4.8×10^6	0.10	0.7	6.9	500.0	10	10	6a, 6b	1,300	1.09×10^{-1}	15.26	140
13	4.8×10^6	0.10	0.6	6.9	500.0	10	10	6e–6f	1,400	1.16×10^{-1}	22.98	199
14	4.8×10^6	0.10	0.7	6.9 ^b	0.0	10	10	7a–7b	4,000	6.78×10^{-2}	14.22	210
14	4.8×10^6	0.10	0.7	6.9 ^b	0.0	10	10	7c–7d	9,000	1.15×10^{-1}	31.14	270
15	4.8×10^6	0.5	0.7	0.0 ^c	0.0	0	0	8a, 8c, 8e	7,500	5.76×10^{-2}	4.31	75
16	4.8×10^6	0.5	0.7	0.0 ^d	0.0	0	0	8b, 8d, 8f	6,000	3.20×10^{-2}	10.88	340
17	4.8×10^6	0.1	0.5	6.9	0.0	10	10	3f	300	5.02×10^{-3}	3.80	1,668

^a Δd , H_d , H_b , t' , and v_{surf} are the nondimensional initial thickness of the dense layer, heat production of the dense material, heat production of less dense material, time, and surface velocity, respectively. Transit time is the estimated time it takes material to traverse the depth of the mantle and is based on surface velocity at the time of the snapshot. The other parameters are described in section 2.

^bCase with a depth-dependent prefactor applied to the viscosity formulation. This prefactor is constant (1) in the upper mantle and jumps to 30 at the upper-lower mantle boundary, below which it linearly increases to 100. The Rayleigh number for this case is based on the upper mantle viscosity.

^cCase with a 50 times less viscous dense layer.

^dCase with a 50 times more viscous dense layer.

where t is time and H is the nondimensional internal heating rate. The equation for chemical advection is

$$\frac{\partial C}{\partial t} + (\mathbf{u} \cdot \nabla)C = 0. \quad (7)$$

The nondimensional temperature and compositionally dependent viscosity is given as

$$\eta(T, C) = \eta_0(r)(1 + \eta_c C)\exp(A(0.5 - T)), \quad (8)$$

where η_0 is a prefactor that may depend on radius, η_c is a constant that allows an intrinsic compositional increase in viscosity, and A is the activation parameter which controls the temperature dependence of viscosity.

2.2. Numerical Method

[12] The convection equations are solved using the finite element code CitcomS [Zhong *et al.*, 2000]. The spherical domain is composed of 12 caps, each containing brick finite elements. The code is parallel, and in these calculations each cap of elements is solved using one processor; however, each cap can be radially subdivided, allowing more processors to be used.

[13] The advection of composition is carried out using tracer particles. Tracers have an advantage over field-based methods, in which numerical diffusion is a problem, and over marker chain methods, which become computationally expensive for complicated flows [van Keken *et al.*, 1997]. We use the ratio tracer method (described and tested by Tackley and King [2003]) which utilizes two sets of tracers, representing each component. Tracer particles are advected using a simple predictor-corrector scheme [e.g., Zhong and Hager, 2003], and the composition of each element is determined by calculating the ratio

of dense tracers to all tracers in a given element. This is the first work utilizing advection of composition in the finite element code CitcomS, and a more detailed description of how the tracers are implemented is given in Appendix A.

[14] Isothermal temperature and free-slip velocity boundary conditions are employed at the top and bottom boundaries. Each cap is composed of 110,592 elements (~ 1.3 million total). The radial direction is spanned by 48 elements. Composition is tracked by 13.5 million tracers. The calculations are started using an initial condition derived from a calculation with a fixed spherical boundary between chemical components.

[15] Given the large number of elements used, we note that the resolution is still not sufficient to provide a quantitatively accurate description of entrainment. This is a typical shortcoming of thermochemical modeling; however, the qualitative feature we study in this work (morphology of a dense layer) is expected to be independent of the exact degree of entrainment [e.g., Tackley, 1998].

3. Results

[16] Table 1 provides a list of parameters used for each calculation and snapshot characteristics for Figures 1–8. Internal heating is applied to the majority of cases, and those cases are characterized by about two thirds of total heat loss generated from internal heating and one third from core heating.

[17] We employed buoyancy ratios within the narrow range between those that lead to immediate overturn and those that lead to a steady, spherical interface, and the ratios used here result in relatively stable layers with significant interface topography. All model calculations experience an initial period of adjustment caused by the initial reduction

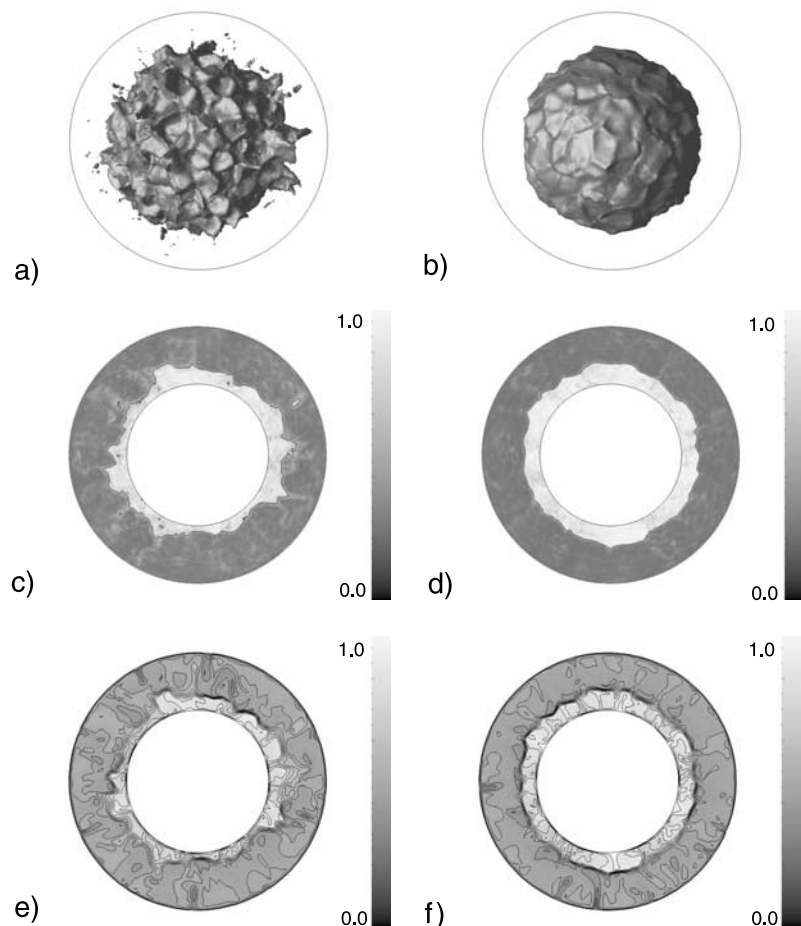


Figure 1. Snapshots from cases 1 and 2 which utilize an isoviscous rheology for calculations with buoyancy ratios 0.7 (Figures 1a, 1c, and 1e) and 0.8 (Figures 1b, 1d, and 1f). (a, b) Compositional isosurface ($C = 0.5$). (c, d) Cross section of compositional field. (e, f) Cross section of temperature field.

of density of the more dense layer (the initial condition calculation employs a high-density lower layer that results in a relatively undeformed interface). The calculations are then run for several thousands of time steps in order to reduce the influence of the initial condition and are usually run until the dense material is fully entrained. It is important to note that this type of thermochemical calculation never obtains an equilibrium condition because of the continual entrainment of material across the interface, and as time increases, both the dense layer thickness and the density contrast across the interface are reduced. This allows us to effectively investigate a continuum series of dense layer thicknesses and density contrasts throughout the duration of a given calculation.

[18] The compositional interface, a slice through the compositional field, and a slice through the thermal field are shown in Figures 1a, 1c, and 1e, respectively, for a calculation which utilizes an isoviscous rheology with a Rayleigh number of 5×10^6 and a buoyancy ratio of 0.7 (case 1). Convection is vigorous in both layers, and there is a large temperature contrast between them. The interface between components is highly deformed, and material is piled and depressed at a local scale. The interface is symmetrical in that deformation along it appears identical

from beneath or above it. Figures 1b, 1d, and 1f are similar snapshots of an isoviscous calculation with a higher buoyancy ratio, $B = 0.8$ (case 2). The increased density contrast results in lower-amplitude deformation along the interface. This set of parameters failed to result in a sweeping of material into rounded piles of material.

[19] Figure 2 shows results from case 3 with a temperature-dependent rheology and a relatively high buoyancy ratio ($B = 0.8$). The rheology provides 3 orders of magnitude difference in viscosity and results in strong, cold slabs and a weak, hot dense layer. This viscosity contrast leads to a surface at the low end of the “sluggish lid” regime. The compositional interface (Figure 2a) experiences only a minor degree of low-amplitude deformation. Examination of the residual temperature (Figure 2b) reveals that the formation of dimples along the interface is caused by the impingement of downwelling material upon it. The dense material is rheologically weak and is easily pushed aside from the downwellings, forming an interconnected series of piled ridges between downwellings. An examination of the calculation animation reveals a dynamic interface in which the dimples migrate across the surface in response to changing positions of downwelling. The logarithm of viscosity is shown in Figure 2c as a slice through the model.

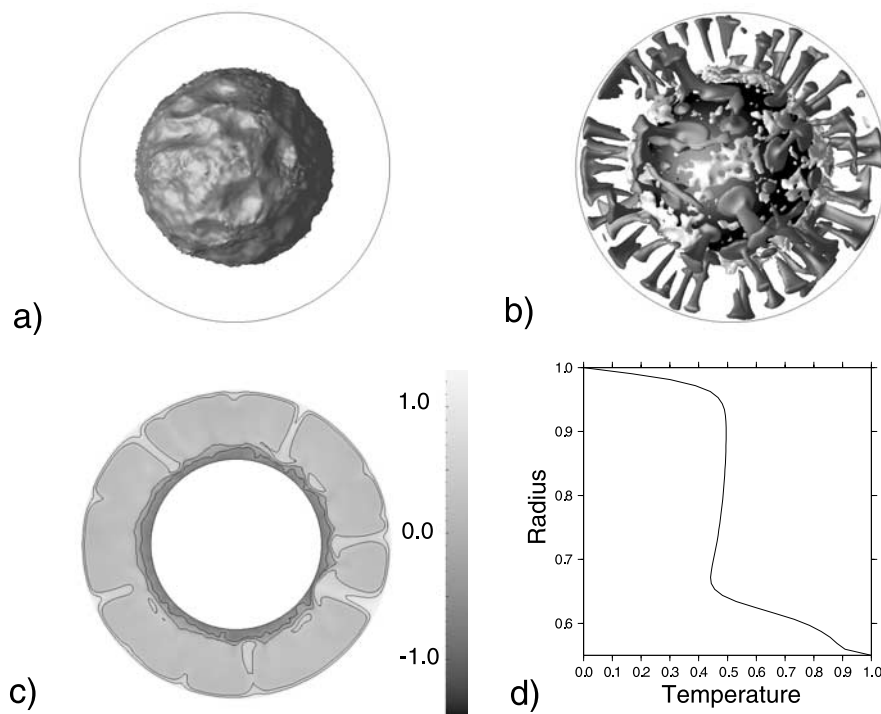


Figure 2. Snapshot of case 3 with temperature-dependent rheology and buoyancy ratio of 0.8. (a) Compositional isosurface ($C = 0.5$). (b) Residual temperature (± 0.15 isotherms). (c) Logarithm of viscosity. (d) Horizontally averaged temperature as a function of radius.

These contours follow the same trend as temperature. The dense layer traps a significant amount of heat, and its temperature is much greater than that of the less dense material. This results in a 2 orders of magnitude decrease in viscosity, making the dense material a passive component in response to the higher-viscosity upper layer. The horizontally averaged radial temperature profile (Figure 2d) illustrates that the dense layer retains a significant amount of heat energy.

[20] Results from a similar temperature-dependent viscosity calculation with a lower buoyancy ratio, $B = 0.7$ (case 4), are shown in Figures 3a–3d. The lower density of the lower layer results in a larger degree of interface topography and a greater ability for downwellings to penetrate through to the core-mantle boundary. The dense material is passively pinched into ridge-like piles that surround the downwellings. Although small dome-like structures sometimes form at the intersections of the ridges, the overall structure of the system is that of interconnected linear ridges that are ubiquitously present, in contrast to isolated, rounded piles.

[21] Decreasing the buoyancy ratio further to $B = 0.6$ (case 5) leads to much greater interface topography (Figure 3e). The dense layer in this calculation does not survive very long and begins to overturn shortly after initiation of the calculation. The general style of deformation along the interface is similar to the cases with higher buoyancy ratios.

[22] We have also performed a set of similar temperature-dependent calculations with a greater dense layer thickness (945 km) (cases 6–8). Compositional fields for these

calculations are shown in Figures 4a–4c for buoyancy ratios 0.8, 0.7, and 0.6, respectively. Comparing these calculations to equivalent cases with a smaller dense layer thickness (Figures 2 and 3), it is observed that increasing the dense layer thickness has little influence on the morphology of the interface between components. Horizontally averaged radial temperature profiles for the three snapshots are shown in Figure 4d. More heat energy is retained in the lowermost mantle for the cases with larger density contrast. We also find that increasing the temperature dependence of viscosity (case 9) and increasing the heat production (case 10) of the dense material does not alter the pattern of linear ridge-like piles forming around downwelling material (Figures 4e and 4f). In fact, we find this pattern prevalent for all cases in which the dense material has a lower viscosity than the less dense material.

[23] Results from a calculation in which an intrinsic increase in viscosity is assigned to the dense component in addition to the temperature dependence are shown in Figure 5. The buoyancy ratio is 0.7, and the dense material is given a factor of 100 increase in viscosity (case 11). We find that this leads to a dramatic change in morphology of the interface. The more viscous dense material plays an active role in convection, as opposed to being passively swept around as in the cases in which the dense material is less viscous. Large plume-like structures of dense material invade the less dense material (Figure 5a). The residual temperature (Figure 5b) reveals large isolated and rounded masses of hotter than average material. Figure 5c shows the logarithm of viscosity. It can be seen that the compositional increase of viscosity neutralizes the

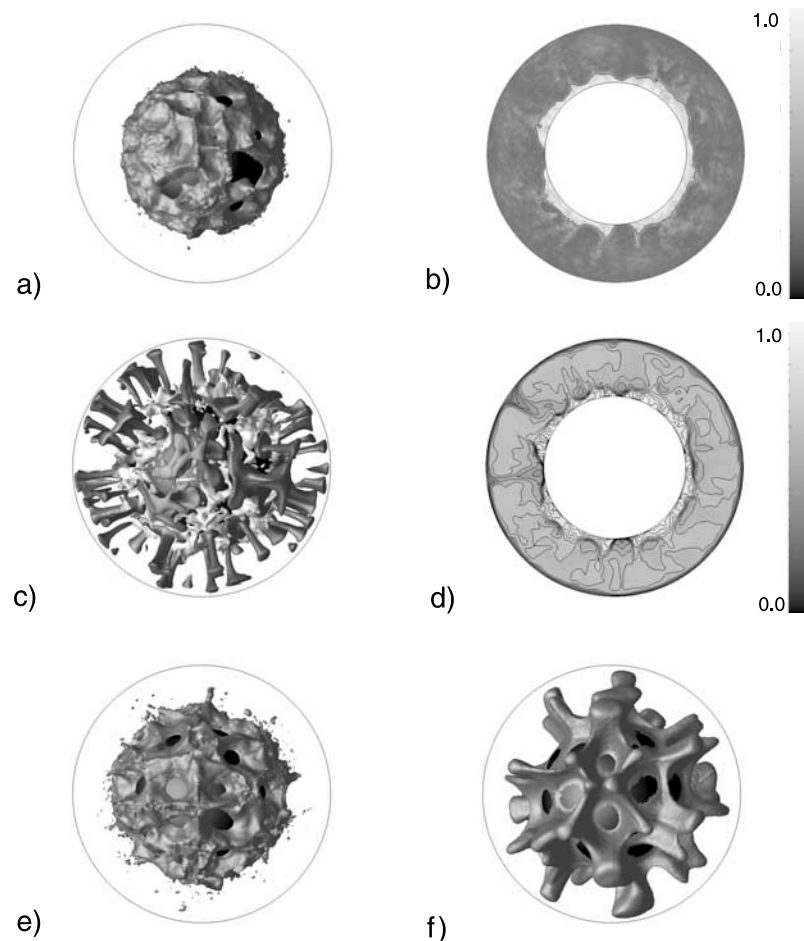


Figure 3. Snapshot of case 4 with temperature-dependent rheology and buoyancy ratio of 0.7. (a) Compositional isosurface ($C = 0.5$). (b) Cross section of compositional field. (c) Residual temperature (± 0.15 isotherms). (d) Cross section of temperature field. (e) Compositional isosurface ($C = 0.5$) of a snapshot of case 5 with temperature-dependent rheology and buoyancy ratio of 0.6. (f) Compositional isosurface ($C = 0.5$) of a snapshot of case 17 with temperature-dependent rheology and buoyancy ratio of 0.5. This latter case is experiencing an initial overturn.

reduction of viscosity because of the temperature dependence in the dense layer, and a high-viscosity rim forms at the interface between components. The dense plumes are dynamic and migrate around the dense layer throughout the calculation. Toward the end of this calculation several of the plumes coalesced into only a few large plumes (Figure 5d).

[24] Figures 6a and 6b show the compositional and residual temperature fields for a case in which the intrinsic compositional increase of viscosity was increased to 500 for the dense material (case 12). The buoyancy ratio is 0.7. Mostly, the large viscosity of the dense material inhibits both convection within the lower layer and the deformation along its interface; however, a single massive, rounded plume formed. Examination of the entire time series indicates that the single plume was formed by two smaller plumes coalescing together.

[25] Maintaining the 500 times viscosity increase while reducing the buoyancy ratio to 0.6 allows a much greater degree of deformation along the interface (Figures 6c–6f, case 13). We find several large, rounded dense plumes

forming and migrating along the density interface. Examination of the temperature slice (Figure 6e) shows that dense layer is too viscous to convect and, for the most part, acts as a thickened thermal boundary layer which cools by forming large plume structures that migrate across the interface.

[26] We also performed a calculation with a constant low-viscosity upper mantle and a lower-mantle viscosity that increases linearly with depth in addition to the temperature dependence (case 14). For a given temperature the bottom of the mantle is 100 times more viscous than the upper mantle. Figures 7a and 7b show the compositional and viscosity fields, respectively, for a given snapshot. The formation of larger-scale structures is observed, likely because of both a reduction of the local Rayleigh number at depth and the radial viscosity profile [Bunge *et al.*, 1996; Zhong *et al.*, 2000]; however, the general style of linear ridges remains. Figures 7c and 7d are snapshots of composition and temperature at a later time in the calculation when the dense material is overturning. It is interesting to note how the piles become

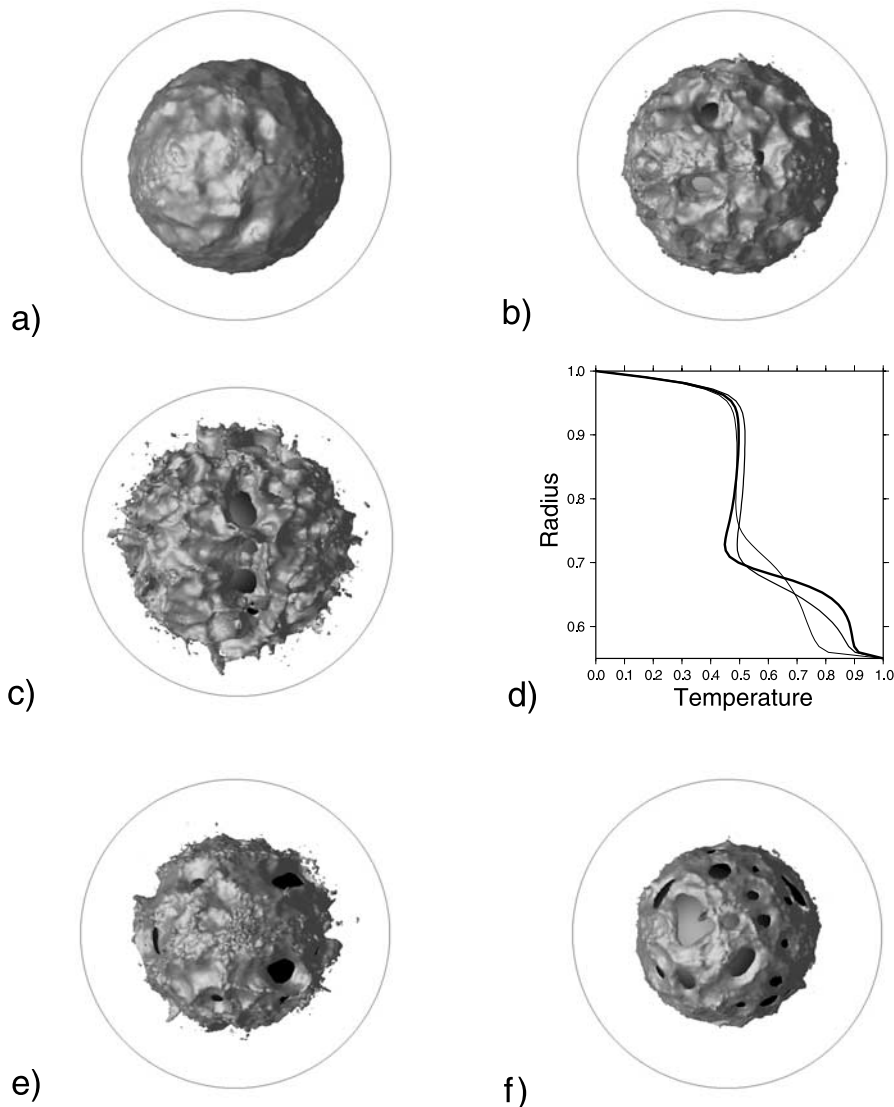


Figure 4. Compositional isosurfaces ($C = 0.5$) for cases 6, 7, and 8 with temperature-dependent rheology and larger dense layer thickness. (a) $B = 0.8$. (b) $B = 0.7$. (c) $B = 0.6$. (d) Horizontally averaged temperature profiles for snapshots shown in Figures 4a–4c (thickest line for Figure 4a and thinnest for Figure 4c). (e) Case 9 which has a higher activation parameter and $B = 0.7$. (f) Case 10 which has a higher dense layer heat production and $B = 0.8$.

more isolated as the volume of dense material decreases, yet they still form ridge-like linear structures.

4. Discussion

[27] Within the parameter range studied here we find that the main control on the morphology of the density interface is the density contrast, which acts to control the amplitude of deformation, and the viscosity ratio of the different components, which acts to control the style of deformation (i.e., ridges versus rounded plumes).

[28] When both viscosities are equivalent, deformation along the interface occurs on a small scale and generates symmetrical structures on both sides of it. Temperature-dependent rheology leads to a weak dense layer because of the higher temperatures of that layer. As a result, the dense

material is passively swept around by downwellings in the less dense material. The weak material is pushed aside by downwellings and is piled up in regions between downwellings. The resultant morphology of the interface is that of an interconnected system of linear ridges which is present ubiquitously throughout the lower mantle. In addition, the network of ridges is not unlike that of thermal ridges formed in purely thermal isochemical convection [Zhong *et al.*, 2000]. Our results indicate that a 3-D spherical geometry with temperature-dependent rheology alone fails to sweep the dense material into isolated, rounded piles. The addition of an intrinsic viscosity increase in the dense material acts to make the dense material an active component with respect to flow. The more viscous dense material forms isolated, rounded plume-like structures that migrate along the interface.

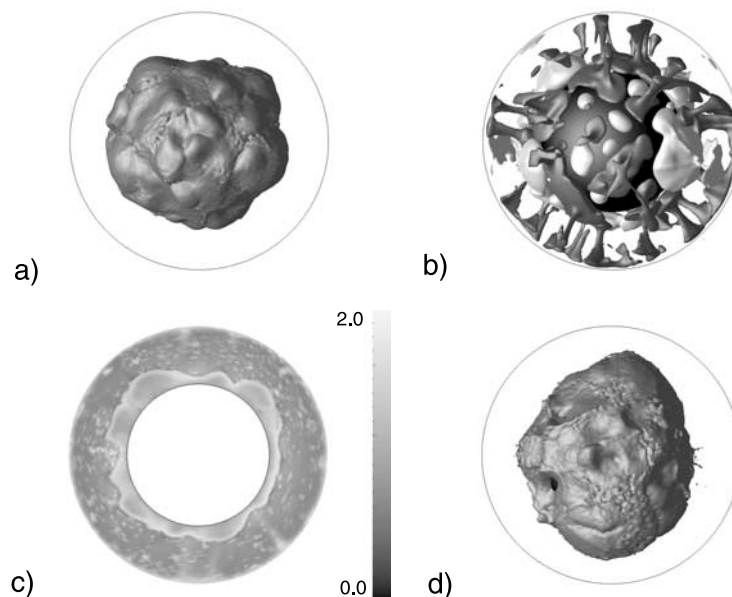


Figure 5. Snapshot of case 11 with both temperature and compositionally dependent rheology. Compositional increase in viscosity is 100 times. $B = 0.7$. (a) Compositional isosurface ($C = 0.5$). (b) Residual temperature (± 0.15 isotherms). (c) Logarithm of viscosity. (d) Compositional isosurface ($C = 0.5$). Results are shown for two times (Figures 5a–5c and Figure 5d).

[29] The difference in morphology between these cases is significant. Figure 8 shows results from a simplified numerical experiment in which the density interface is placed at midmantle depth. Both cases employ purely compositionally dependent rheology. Figures 8a, 8c, and 8e show the compositional, temperature, and residual temperature fields, respectively, for a case in which the dense material is 50 times less viscous (case 15). Figures 8b, 8d, and 8f show the same fields for a case in which the dense material is 50 times more viscous (case 16). It is observed that the more viscous layer is the more active one in terms of imposing its flow structure. In the case with the lower (higher) viscosity dense layer it is the downwellings (upwellings) of the upper (lower) layer which push around the more passive dense (less dense) material. Comparing the compositional fields (Figures 8a and 8b), it is clear that the deformation for one case is simply the inverse of the other. The more viscous material encroaches into the less viscous material by means of large plume structures.

[30] We find that the spherical geometry alone does not significantly influence the morphology of the density interface. In fact, the general style of deformation resembles that observed in 3-D Cartesian numerical and laboratory studies. Our cases with only temperature-dependent rheology, resulting in a weak dense component, produce structures similar to those observed in the laboratory work of *Jellinek and Manga* [2002]. The “circular embayments” and “divides” they observe closely resemble the circular regions in our study where dense material is swept away from downwellings and the ridge-like piles where dense material is pushed toward downwellings. *Jellinek and Manga* [2002] do not give an explanation for these structures, but it is feasible to surmise that they are caused by material being passively swept by downwellings, as in our study. We also find that the structures observed in our

study (for temperature-dependent rheology) resemble those observed by *Tackley* [2002] where he studied the effect of a weak dense layer. He also observed a ridge-like network of piles of dense material.

[31] The studies of *Davaille* [1999] and *Davaille et al.* [2002, 2003] primarily maintain the dense layer as the more viscous one, and we propose that the rounded, dense plumes observed in our cases with a higher-viscosity dense layer are similar structures to *Davaille et al.*’s domes, which they suggest may be superplumes. The large plume structures observed in our study oscillate, as *Davaille et al.* observe; however, the mode of oscillation is different. *Davaille*’s group’s studies indicate that the domes rise and then either mix with the less dense material or cool and vertically descend to the bottom of the tank. The plume structures in our study oscillate by migrating around the lower mantle; hence a particular region in space experiences a vertical rising and sinking. However, the viscous plumes are long-lived and are laterally mobile.

[32] In addition, *Davaille*’s group observes not only that the direction of doming is related to the tendency for viscous material to dome into less viscous material (as we observe) but also that there is a preference for the thinner layer to dome into the thicker layer. Therefore they state that a thin layer of less viscous material can dome into more viscous material [*Davaille et al.*, 2003]. We do not observe this in our calculations, but we put forth a possible explanation. Our study emphasizes systems in which the dense layer is relatively stable for long periods of time; however, we have performed calculations in which the dense material is initially unstable. In these initially unstable cases the dense material does rise into the upper mantle in domes, even for cases in which the dense material is less viscous. Figure 3f shows a snapshot of an initial overturn in which the dense material is less viscous and the buoyancy ratio is

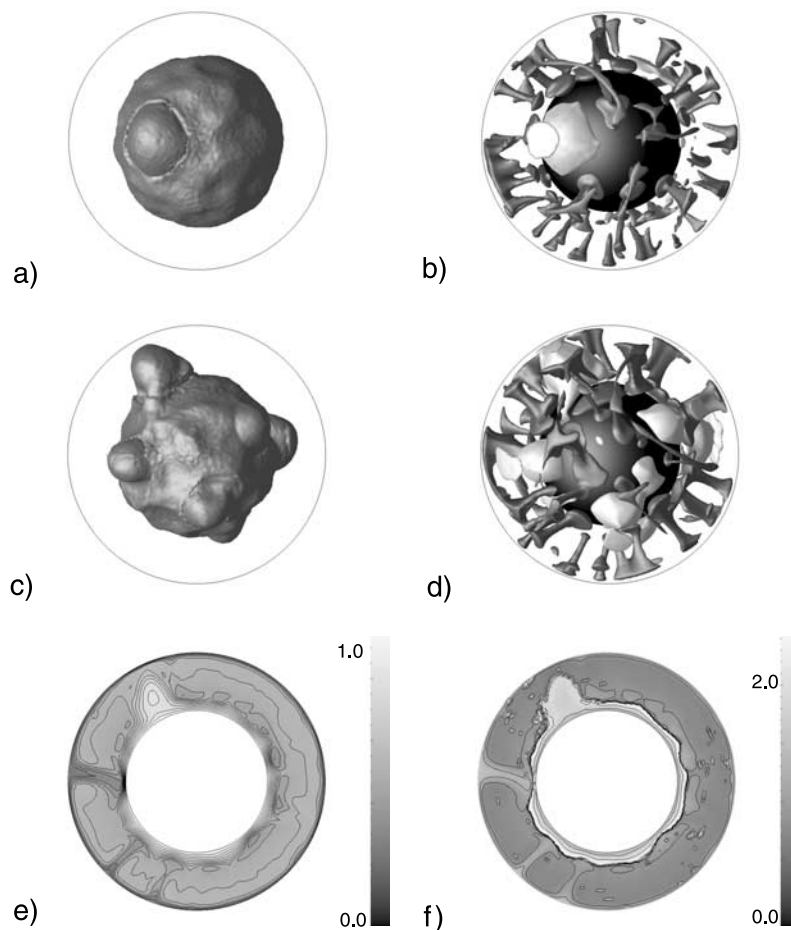


Figure 6. Snapshots of case 12 with both temperature-dependent and compositionally dependent rheology (Figures 6a and 6b). Compositional increase in viscosity is 500 times. $B = 0.7$. (a) Compositional isosurface ($C = 0.5$). (b) Residual temperature (± 0.15 isotherms). Snapshot of case 13 with both temperature- and composition-dependent rheology (Figures 6c–6f). Compositional increase in viscosity is 500 times. $B = 0.6$. (c) Compositional isosurface ($C = 0.5$). (d) Residual temperature (± 0.15 isotherms). (e) Cross section of temperature field. (f) Cross section of the logarithm of the viscosity field.

0.5. The less viscous material domes into the upper mantle, cools, and sinks, similar to the experiments of *Davaille et al.* [2003]. In this calculation the dense material rapidly mixes with less dense material upon descent, and whole mantle convection quickly ensues. This is in agreement with *Davaille et al.*'s observation that their domes undergo a finite number of oscillations before complete mixing.

[33] Our work suggests that doming structures can form within material of higher or lower viscosity when experiencing an overturn leading to complete mixing, and these domes move in a vertical fashion. However, for relatively stable dense layers, as studied here, only those with higher viscosity produce long-lived dome structures that migrate throughout the lower mantle.

[34] The results from this work indicate that there is a distinction between thermochemical structures that are piles versus those that are superplumes. We propose that if a dense component does not have an intrinsic viscosity increase, temperature-dependent rheology leads to it being weaker and more passive; therefore it is passively swept into linear piles. These linear ridge-like piles are numerous and should be observed ubiquitously throughout the lower

mantle. An intrinsic viscosity increase, however, allows the dense material to flow actively, forming a small number of isolated, rounded superplume structures that are long-lived and migrate across the lower mantle. For the parameter range studied here these structures are mutually exclusive, and a dense component will either exhibit linear ridge-like piles or rounded superplumes, depending on whether there is an intrinsic viscosity contrast between components.

[35] Again, we note that this study concentrates on thermochemical convection with a relatively stable dense layer. If there is a dense component in the lower mantle and if it is in a transient state of overturn, the structures produced will likely be complicated and varied in appearance. We are therefore hesitant to conclude from this study that some seismic observations that hint at rounded regions of chemical heterogeneity [e.g., *Ishii and Tromp*, 1999; *Masters et al.*, 2000] are indicative of the presence of a more viscous dense component above the CMB. There are still difficulties associated with models involving a dense layer, particularly in terms of the large temperature contrast between components, but if there is a dense component of significant thickness present in the lower mantle, its morphology should give us insight into the

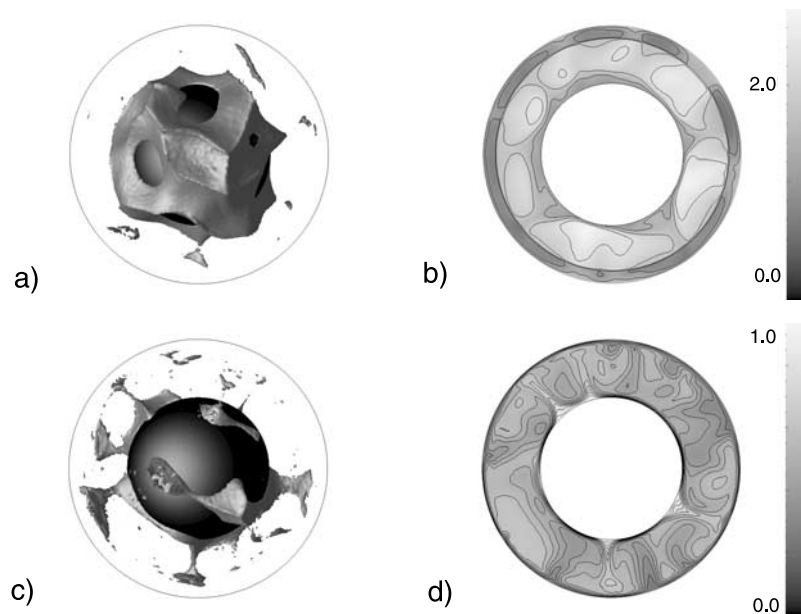


Figure 7. Snapshots of case 14 with a radial dependence of viscosity in addition to temperature dependence. Viscosity of upper mantle is 1, whereas in the lower mantle, viscosity increases from 30 to 100 times with depth. (a) Compositional isosurface ($C = 0.5$) at an earlier time. (b) Logarithm of viscosity. (c) Compositional isosurface ($C = 0.5$) at a later time. (d) Cross section of temperature field. Snapshots are shown for two times (Figures 7a and 7b and Figures 7c and 7d).

rheology of that material. Normal temperature-dependent rheology is expected to produce linear ridges all throughout the lower mantle, not simply in a few isolated regions such as the Pacific and Africa. If observations do indeed exclude a ubiquitous presence of another chemical component and show that it is in the form of rounded superplumes under only a small number of locations, it is likely that the dense material either has a higher viscosity or is in a state of overturn.

[36] We have not addressed the issue of layer stability in this study, which has both numerical and scientific difficulties associated with it. It has been well recognized that the numerical treatment of thermochemical convection is insufficient to accurately quantify entrainment of material at grid resolutions presently possible given the present computing power [van Keken *et al.*, 1997]; however, numerical calculations are able to adequately capture the qualitative aspects of thermochemical convection, such as flow structure and general appearance [Tackley, 1998]. In general, thermochemical convection never reaches a steady state condition, and investigating the long-term stability of a dense layer requires a quantitative understanding of entrainment [Sleep, 1988; Davaille, 1999; Gonnermann *et al.*, 2002; Zhong and Hager, 2003] because through time, one component is continually being entrained into the other and, as a result, both the density contrast and dense layer thickness decrease as a function of time. The buoyancy ratio used in numerical calculations is effectively an initial density contrast, and the effective buoyancy number decreases with time. In addition, as the less dense layer is depleted, the effective Rayleigh number increases, leading to increased convective vigor with time. We have discovered that at grid resolutions tenable today, entrainment is typically enhanced, leading to a more rapid destruction of a dense component. It is therefore not practical

to conclude anything about long-term stability of a dense layer under a given set of parameters in this study. We merely investigate the general behavior of the thermochemical system for a given rheology. Moreover, lack of knowledge of the appropriate initial condition, particularly the temperature profile, precludes an adequate investigation of long-term stability. A dense layer that is initially too hot, as is often the case when beginning the calculation with a thermal equilibrium condition from a calculation with a fixed density interface, may have a transient period of heavy mixing or may even overturn quickly, whereas a cooler start would lead to a long-lived layer.

[37] For the isoviscous and temperature-dependent cases we were able to investigate different layer thicknesses. As the calculation time increased, the dense layer thickness decreased because of entrainment. In addition, entrainment also leads to a reduction of density contrast, so as a given calculation proceeds, we are effectively investigating a continuum of dense layer thicknesses and buoyancy ratios. We observed that the thermochemical structures remained similar throughout a given calculation, although their size was reduced and the amplitude of deformation increased (compare Figures 7a and 7c). Both isoviscous and temperature-dependent cases were characterized by passive linear ridge segments throughout the duration of the calculation. We were not able to investigate this for the compositionally dependent cases because the viscous film generated between the two layers significantly reduced entrainment, and it is not clear if thinner dense layers would lead to a different style of deformation in these cases. It is likely, however, that a thinner viscous layer would simply lead to a conductive boundary layer at the base of the mantle.

[38] We point out the necessity of 3-D studies to investigate the morphology of a dense component. Two-dimensional

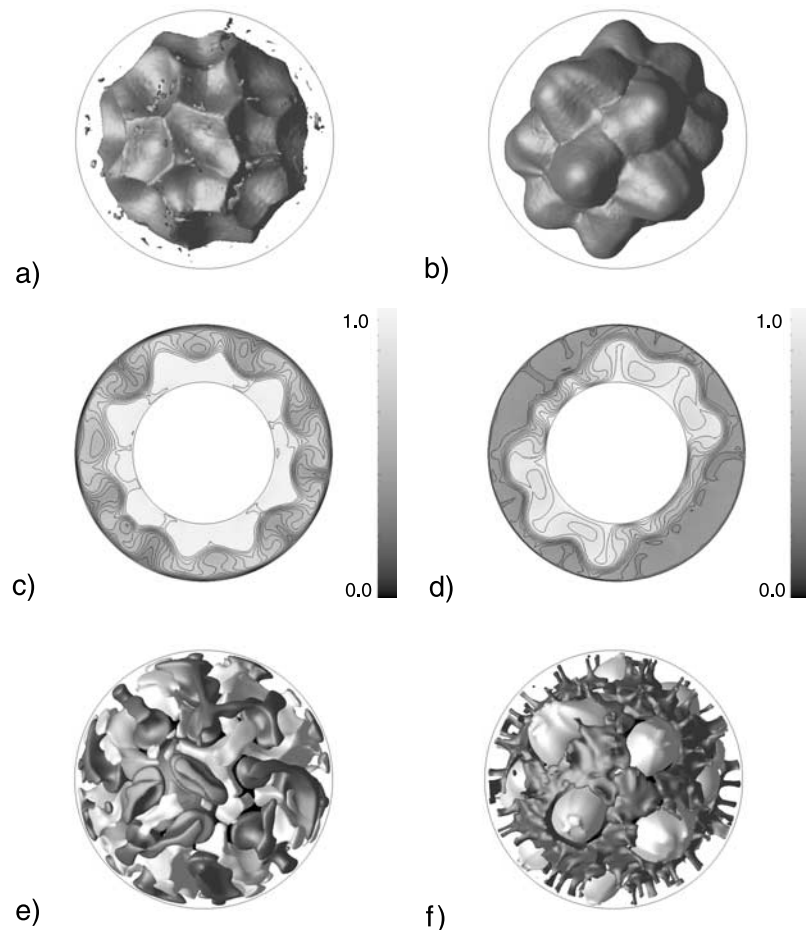


Figure 8. Snapshots of cases 15 and 16, one with a 50 times lower viscosity in the dense layer (Figures 8a, 8c, and 8e) and the other with a 50 times higher viscosity in the dense layer (Figures 8b, 8d, and 8f). (a, b) Compositional isosurface ($C = 0.5$). (c, d) Cross section of temperature field. (e, f) Residual temperature (± 0.15 isotherms).

studies often reveal the presence of piled material, yet they fail to distinguish between rounded and linear structures. Even in cross section of 3-D models, it is difficult to discern between rounded superplumes and linear piles, although the inflection of the interface may give some clue. We also point out the importance of rheology in this type of study. Comparison of the temperature-dependent rheology cases with those having only isoviscous rheology indicates a significant difference in structure. We find that although isoviscous modeling is much more attractive in terms of computational expense, it is not appropriate for trying to understand the morphology of a proposed dense layer in the Earth.

[39] It should be noted from Table 1 that surface velocities are roughly 1 order of magnitude lower than that of the Earth. We employed Rayleigh numbers a little lower than Earth-like to reduce the computational cost, which in turn, allowed us to search a more useful parameter range. We expect the general character of the thermochemical convection to be similar for more realistic Rayleigh numbers.

[40] These calculations were performed using the Boussinesq approximation, which lacks more Earth-like characteristics such as compressibility, adiabatic heating/

cooling, viscous dissipation, and depth-dependent thermodynamic properties. It is likely that inclusion of depth-dependent properties would lead to larger length scales of convection [Tackley, 1996a, 1996b]. It should be noted that while depth-dependent parameters may act to increase the length scale of convection, increasing the Rayleigh number to more realistic values would act to reduce the length scale. The calculation that included depth-dependent viscosity (case 14) was performed in order to investigate whether the style of deformation would remain the same as the length scale was increased. The thermochemical structures produced were much larger in scale; however, their linear ridge-like morphology remained. We propose that the scale and style of deformation is decoupled; however, future work involving more complicated extended Boussinesq thermochemical models along with more Earth-like Rayleigh numbers would be needed to confirm this.

[41] It is important to note that our study does not include plate tectonics which may alter the overall flow structure. It is conceivable that long-lived regions of subduction may focus the dense component differently than shown here, but precursory work has indicated that it is unlikely that the presence of plates would dramatically alter the conclusions

Table A1. Tracer Resolution Test^a

Elements	dt (Time Steps)	r_f	θ_f	ϕ_f	Difference	Difference/Length
Second-order Runge-Kutte	4.858×10^{-7} (200,000)	0.90680	1.45465	2.00000		
393,216	10^{-4} (200)	0.90676	1.45474	1.99965	0.00033	0.02%
1,327,104	10^{-4} (200)	0.90679	1.45469	1.99986	0.00013	0.008%

^aVariables r_f , θ_f , and ϕ_f refer to final coordinates of tracer originating at (0.55, 1.0, 0.0). Difference/length is the percentage error to the tracer's total path length, which is ~ 3.3 mantle thicknesses.

of this study. Trying to include plate tectonics in convection models is fraught with difficulty, but work involving imposing time-evolving plate velocities at the surface of the model is currently being initiated in order to investigate the effect of plate motions on a hypothetical dense component in the Earth's lower mantle.

5. Conclusions

[42] We performed a numerical study to investigate the style of structures formed in a mantle containing a moderate amount of dense material in the lower mantle. In particular, we investigate whether a spherical geometry acts to focus the dense material into a few isolated, rounded piles, as inferred from recent seismic studies. Our study shows that spherical geometry alone fails to focus material into rounded piles, and features observed in this study compare relatively well with those from 3-D Cartesian numerical and laboratory studies. We find that the main control on how the dense material is organized is the viscosity contrast between components. Purely temperature-dependent rheology leads to a weaker dense layer which is passively swept by downwellings into a network of linear ridge-like piles which are ubiquitously present in the lower mantle. The addition of an intrinsic viscosity increase in the dense material causes it to flow more actively, generating a small number of large superplume structures that are long-lived and migrate around the lower mantle.

[43] We find that piles and superplumes are separate features and generally do not occur together, at least under the set of parameters studied here. As seismic coverage of proposed chemical components in the lower mantle is increased, it may be possible to better understand the rheology of a proposed dense component by observing the geometry of the interface.

Appendix A: Tracer Method

[44] The most challenging aspect of composition advection in a non-Cartesian model such as CitcomS is tracking particles and interpolating their velocity from nearby nodal points. For a given tracer coordinate, (r , θ , ϕ), it is important to locate the element that the tracer is in, and Cartesian models typically employ element grids aligned in directions parallel to the coordinate system axes. Spherical models such as CitcomS [Zhong *et al.*, 2000], however, utilize an element grid composed of brick elements which are aligned to only the \hat{r} axis. It is trivial to find the radial shell a tracer belongs to; however, the element within a given shell is not easily found by knowing its azimuthal position.

[45] The element that a given tracer belongs to is determined by vector operations. Each surface edge of an

element can be viewed as a vector between two nodes, and another vector can be constructed from the end of that vector to the tracer in question. If the resultant cross products of these two vectors are positive in the radial direction for every surface edge of the element, the tracer is determined to be inside of that element. The computational cost of performing these operations for each tracer over all the elements is extremely costly, but we circumvent this problem by laying down a finer regular grid over the CitcomS grid. The regular grid is composed of elements with sides aligned to the spherical coordinates θ and ϕ , and the lengths of these element boundaries are of constant intervals ($\Delta\theta$, $\Delta\phi$). It is trivial to find which regular element a tracer with given spherical coordinates belongs to. The regular grid is made fine enough that most regular elements are completely encompassed within a CitcomS brick element, and the mapping of the finer regular elements to CitcomS elements needs to only be performed once using cross-product calculations. A somewhat different yet similar procedure has been found to work extremely well for 2-D cylindrical models with irregular grids of triangular elements [van Keken and Ballentine, 1998; McNamara *et al.*, 2003] and for passive particle tracing in CitcomS [van Keken and Zhong, 1999].

[46] A tracer's velocity is determined by interpolation from elemental nodal points using linear shape functions [Cuvelier *et al.*, 1986; Hughes, 1987]; however, a tracer's local coordinates (ξ , η , ζ) must first be determined from global coordinates (θ , ϕ , r). This mapping is trivial only in the radial direction. The radial and azimuthal shape functions are decoupled, and the task is to find local coordinates and shape functions in the remaining two-dimensional azimuthal slice. We transform the azimuthal coordinates of nodes and tracers into a space in which great circles become straight lines (gnomonic projection), which allows the elements to become straight edged, and the resultant azimuthal slice is conveniently split into two triangles, allowing standard linear shape functions to be used.

[47] We use a simple predictor-corrector method to propagate the tracers with time similar to that described by Zhong and Hager [2003]. We tested the tracer method by assigning the following analytical flow field:

$$\mathbf{V} = 25r\hat{r} + 50r \cos(\phi)\hat{\theta} + 100r \sin(\theta)\hat{\phi}. \quad (\text{A1})$$

We calculated the trajectory of a tracer independently with a second-order Runge-Kutte scheme with very small time steps to compare to our CitcomS tracing. The nondimensional velocity, radius, and time for this tracer test are based on a length scale nondimensionalization based on Earth radius rather than mantle thickness.

[48] The initial position of a particle is set at

$$(r, \theta, \phi) = (0.55, 1.0, 0.0), \quad (\text{A2})$$

and the calculation is run for 200 time steps, which corresponds to a Courant time typical for these velocities and resolutions ($\sim 10^{-4}$). Results are shown in Table A1, and we are confident that the error is small enough for the type of study performed here.

Appendix B: Resolution Tests

[49] The calculations presented in this work are performed on a mesh of ~ 1.3 million elements, which makes these calculations computationally expensive. The grid resolution used in the calculations for this study is at a practical maximum. Higher resolutions are possible but at a trade-off of searching a smaller parameter range. We realize that numerical modeling of thermochemical convection at this grid resolution does not allow us to quantitatively measure the proper degree of entrainment, and we find that the rate of entrainment, and therefore the longevity of a dense layer, is dependent on resolution. However, we find that the resolution used here does adequately capture the general style of convection and deformation of the density interface.

[50] We have performed several resolution tests in order to ensure that we are reproducing the correct style of deformation in our calculations. Our tests involve increasing the number of tracers, increasing the resolution, and decreasing the time step. The control set of parameters is that used in the calculation shown in Figure 3 (i.e., case 4 with temperature-dependent rheology, $B = 0.7$, and 1.3 million tracers), and the cases shown in Figure B1 should be compared to Figures 3a and 3c. Figure B1a shows the compositional field of a case in which we doubled the number of tracers from ~ 13 to ~ 26 million. We find no significant difference in the pattern of convection or style of deformation along the density interface. In addition, the amount of entrainment over time is similar to that of the control case.

[51] Figure B1b shows a similar snapshot for a calculation in which the resolution was increased to ~ 3.1 million elements. We find that this increased resolution leads to the same general style as the control case with perhaps a little less topography along the interface. We find that the increased resolution has a significant impact upon entrainment rates, and the higher resolution leads to less entrainment and therefore longer-lived stable dense layers. This has also been observed by *Tackley and King* [2003]. We conclude that the control case generates the same style of features along the interface and the same general flow pattern as the higher-resolution case, so resolutions used in this work are deemed adequate. If we wanted to study entrainment and long-term survivability of a dense layer, we would have to increase our grid resolution.

[52] In order to test the conservation of composition in our models we plot the compositional error fraction as a function of time for the four test cases (Figure B1c). This fraction is defined as the fractional change in the dense component volume with respect to its initial volume. We observe that in our calculations the volume of dense

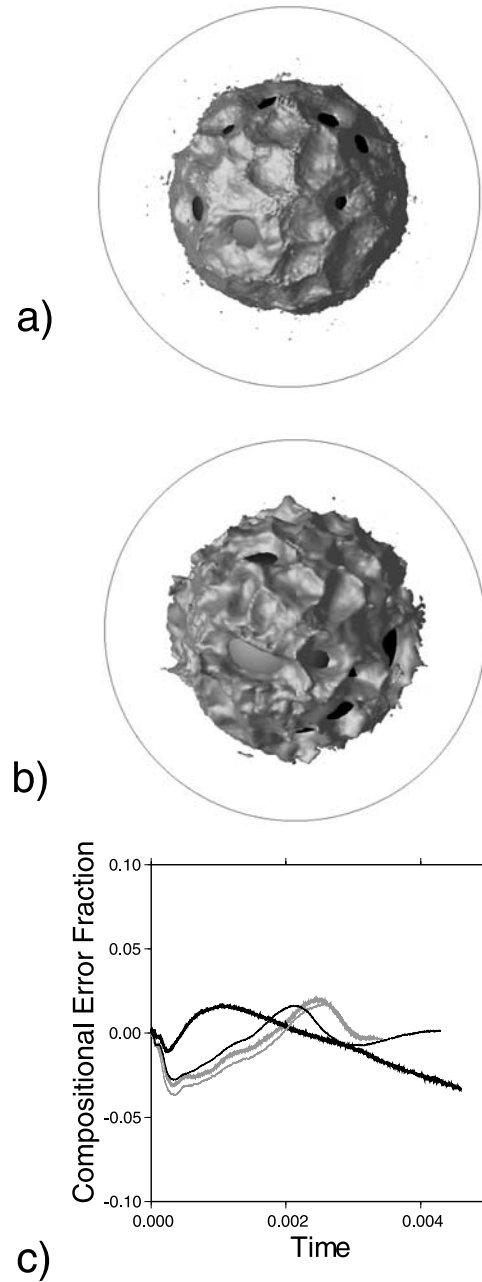


Figure B1. Results from resolution tests. (a) Twice as many tracers; compositional isosurface ($C = 0.5$). (b) Higher resolution; compositional isosurface ($C = 0.5$). (c) Compositional error fraction as a function of time for four resolution tests: (1) control case (thick shaded line), (2) higher resolution (thick solid line), (3) smaller time step (thin shaded line), and (4) twice as many tracers (thin solid line).

material typically oscillates within 3% of its original volume. While this is not optimal for detailed calculations of entrainment, this error does not affect the type of study performed here.

[53] **Acknowledgments.** We thank Paul Tackley and Ctirad Matyska for careful and insightful reviews. This work is supported by the David and Lucile Packard Foundation and NSF under grant EAR 0134939.

References

- Becker, T. W., J. B. Kellogg, and R. J. O'Connell (1999), Thermal constraints on the survival of primitive blobs in the lower mantle, *Earth Planet. Sci. Lett.*, *171*, 351–365.
- Bijwaard, H., W. Spakman, and E. R. Engdahl (1998), Closing the gap between regional and global travel time tomography, *J. Geophys. Res.*, *103*, 30,055–30,078.
- Bunge, H.-P., M. A. Richards, and J. R. Baumgardner (1996), Effect of depth-dependent viscosity on the planform of mantle convection, *Nature*, *379*, 436–438.
- Cuvelier, C., A. Segal, and A. A. van Steenhoven (1986), *Finite Element Methods and Navier-Stokes Equations*, D. Reidel, Norwell, Mass.
- Davaille, A. (1999), Simultaneous generation of hotspots and superswells by convection in a heterogeneous planetary mantle, *Nature*, *402*, 756–760.
- Davaille, A., F. Girard, and M. Le Bars (2002), How to anchor hotspots in a convecting mantle?, *Earth Planet. Sci. Lett.*, *203*, 621–634.
- Davaille, A., M. Le Bars, and C. Carbonne (2003), Thermal convection in a heterogeneous mantle, *Geodynamics*, *335*, 141–156.
- Davies, G. F., and M. A. Richards (1992), Mantle convection, *J. Geol.*, *100*, 151–206.
- Gonnermann, H. M., M. Manga, and A. M. Jellinek (2002), Dynamics and longevity of an initially stratified mantle, *Geophys. Res. Lett.*, *29*(10), 1399, doi:10.1029/2002GL014851.
- Grand, S. P., R. D. van der Hilst, and S. Widiyantoro (1997), Global seismic tomography: A snapshot of convection in the Earth, *GSA Today*, *7*, 1–7.
- Hofmann, A. W. (1997), Mantle geochemistry: The message from oceanic volcanism, *Nature*, *385*, 219–229.
- Hughes, T. J. R. (1987), *The Finite Element Method*, Prentice-Hall, Old Tappan, N. J.
- Ishii, M., and J. Tromp (1999), Normal-mode and free-air gravity constraints on lateral variation in velocity and density of Earth's mantle, *Science*, *285*, 1231–1236.
- Jellinek, A. M., and M. Manga (2002), The influence of a chemical boundary layer on the fixity, spacing, and lifetime of mantle plumes, *Nature*, *418*, 760–763.
- Kellogg, L. H., B. H. Hager, and R. D. van der Hilst (1999), Compositional stratification in the deep mantle, *Science*, *283*, 1881–1884.
- Masters, G., G. Laske, H. Bolton, and A. Dziewonski (2000), The relative behavior of shear velocity, bulk sound speed, and compressional velocity in the mantle: Implications for chemical and thermal structure, in *Earth's Deep Interior: Mineral Physics and Tomography From the Atomic to the Global Scale*, *Geophys. Monogr. Ser.*, vol. 117, edited by S. Karato et al., pp. 63–87, AGU, Washington, D. C.
- McNamara, A. K., and P. E. van Keken (2000), Cooling of the Earth: A parameterized convection study of whole versus layered models, *Geochem. Geophys. Geosyst.*, *1*, Paper number 2000GC000045.
- McNamara, A. K., P. E. van Keken, and S.-I. Karato (2003), Development of finite strain in the convecting lower mantle and its implications for seismic anisotropy, *J. Geophys. Res.*, *108*(B5), 2230, doi:10.1029/2002JB001970.
- McNutt, M. K. (1998), Superswells, *Rev. Geophys.*, *36*, 211–244.
- Meibom, A., D. L. Anderson, N. H. Sleep, R. Frei, C. P. Chamberlain, M. T. Hren, and J. L. Wooden (2003), Are high $^3\text{He}/^4\text{He}$ ratios in oceanic basalts an indicator of deep-mantle plume components?, *Earth Planet. Sci. Lett.*, *208*, 197–204.
- Ni, S., and D. V. Helmberger (2003a), Ridge-like lower mantle structure beneath South Africa, *J. Geophys. Res.*, *108*(B2), 2094, doi:10.1029/2001JB001545.
- Ni, S., and D. V. Helmberger (2003b), Seismological constraints on the South African superplume: Could be the oldest distinct structure on Earth, *Earth Planet. Sci. Lett.*, *206*, 119–131.
- Ni, S., E. Tan, M. Gurnis, and D. Helmberger (2002), Sharp sides to the African superplume, *Science*, *296*, 1850–1852.
- Olson, P. (1984), An experimental approach to thermal convection in a two-layered mantle, *J. Geophys. Res.*, *89*, 11,293–11,301.
- Olson, P., and C. Kincaid (1991), Experiments on the interaction of thermal convection and compositional layering at the base of the mantle, *J. Geophys. Res.*, *96*, 4347–4354.
- Romanowicz, B., and Y. Gung (2002), Superplumes from the core-mantle boundary to the lithosphere: Implications for heat flux, *Science*, *296*, 513–516.
- Sleep, N. H. (1988), Gradual entrainment of a chemical layer at the base of the mantle by overlying convection, *Geophys. J. Int.*, *95*, 437–447.
- Spohn, T., and G. Schubert (1982), Modes of mantle convection and the removal of heat from the Earth's interior, *J. Geophys. Res.*, *87*, 4682–4696.
- Su, W., and A. M. Dziewonski (1997), Simultaneous inversion for 3-D variations in shear and bulk velocity in the mantle, *Phys. Earth Planet. Inter.*, *100*, 135–156.
- Tackley, P. J. (1996a), On the ability of phase transitions and viscosity layering to induce long-wavelength heterogeneity in the mantle, *Geophys. Res. Lett.*, *23*, 1985–1988.
- Tackley, P. J. (1996b), Effects of strongly variable viscosity on three-dimensional compressible convection in planetary mantles, *J. Geophys. Res.*, *101*, 3311–3332.
- Tackley, P. J. (1998), Three-dimensional simulations of mantle convection with a thermo-chemical basal boundary layer: D^{''}?, in *The Core-Mantle Boundary Region*, *Geodyn. Ser.*, vol. 28, edited by M. Gurnis et al., pp. 231–253, AGU, Washington, D. C.
- Tackley, P. J. (2002), Strong heterogeneity caused by deep mantle layering, *Geochem. Geophys. Geosyst.*, *3*(4), 1024, doi:10.1029/2001GC000167.
- Tackley, P. J., and S. D. King (2003), Testing the tracer ratio method for modeling active compositional fields in mantle convection simulations, *Geochem. Geophys. Geosyst.*, *4*(4), 8302, doi:10.1029/2001GC000214.
- van der Hilst, R. D., and H. Karason (1999), Compositional heterogeneity in the bottom 1000 kilometers of the Earth's mantle: Toward a hybrid convection model, *Science*, *283*, 1885–1888.
- van der Hilst, R. D., S. Widiyantoro, and E. R. Engdahl (1997), Evidence for deep mantle circulation from global tomography, *Nature*, *386*, 579–584.
- van Keken, P., and C. J. Ballentine (1998), Whole-mantle versus layered mantle convection and the role of a high viscosity lower mantle in terrestrial volatile evolution, *Earth Planet. Sci. Lett.*, *156*, 19–32.
- van Keken, P., and S. Zhong (1999), Mixing in a 3D spherical model of present-day mantle convection, *Earth Planet. Sci. Lett.*, *171*, 533–547.
- van Keken, P. E., S. D. King, H. Schmeling, U. R. Christensen, D. Neumeister, and M.-P. Doin (1997), A comparison of methods for the modeling of thermochemical convection, *J. Geophys. Res.*, *102*, 22,477–22,496.
- Zhong, S., and B. H. Hager (2003), Entrainment of a dense layer by thermal plumes, *Geophys. J. Int.*, *154*, 666–676.
- Zhong, S., M. T. Zuber, L. Moresi, and M. Gurnis (2000), Role of temperature-dependent viscosity and surface plates in spherical shell models of mantle convection, *J. Geophys. Res.*, *105*, 11,063–11,082.

A. K. McNamara and S. Zhong, Department of Physics, University of Colorado, 390 UCB, Boulder, CO 80309-0390, USA. (mcnamar@colorado.edu; szhong@spice.colorado.edu)